



OPEN

SUBJECT AREAS:
CANCER IMAGING
TRANSLATIONAL RESEARCH
MAGNETIC RESONANCE
IMAGINGReceived
20 August 2014Accepted
10 November 2014Published
1 December 2014Correspondence and
requests for materials
should be addressed to
W.W. (wangwen@
fmmu.edu.cn) or G.C.
(cgbtd@126.com)* These authors
contributed equally to
this work.

Intravoxel incoherent motion diffusion-weighted MR imaging of gliomas: efficacy in preoperative grading

Yu-Chuan Hu^{1*}, Lin-Feng Yan^{1*}, Lang Wu^{2*}, Pang Du¹, Bao-Ying Chen¹, Liang Wang³, Shu-Mei Wang⁴, Yu Han¹, Qiang Tian¹, Ying Yu¹, Tian-Yong Xu⁵, Wen Wang⁶ & Guang-Bin Cui¹

¹Department of Radiology, Tangdu Hospital, Fourth Military Medical University, Xi'an, Shaanxi, P.R. China, ²Center for Clinical and Translational Science, Mayo Clinic, Rochester, Minnesota, USA, ³Department of Neurosurgery, Tangdu Hospital, Fourth Military Medical University, Xi'an, Shanxi, P.R. China, ⁴Department of Pathology, Tangdu Hospital, Fourth Military Medical University, Xi'an, Shanxi, P.R. China, ⁵MR Research China, GE healthcare Greater China, Beijing, China, ⁶Department of Anatomy & K.K. Leung Brain Research Centre, Fourth Military Medical University, Xi'an, Shaanxi, PR China.

The preoperative grading of gliomas, which is critical for guiding therapeutic strategies, remains unsatisfactory. We aimed to retrospectively assess the efficacy of intravoxel incoherent motion (IVIM) diffusion-weighted imaging (DWI) in the grading of gliomas. Forty-two newly diagnosed glioma patients underwent conventional MR imaging, DWI, and contrast-enhanced MR imaging. Parameters of apparent diffusion coefficient (ADC), slow diffusion coefficient (D), fast diffusion coefficient (D*), and fraction of fast ADC (f) were generated. They were tested for differences between low- and high-grade gliomas based on one-way ANOVA. Receiver-operating characteristic (ROC) analyses were conducted to determine the optimal thresholds as well as the sensitivity and specificity for grading. ADC, D, and f were higher in the low-grade gliomas, whereas D* tended to be lower (all $P < 0.05$). The AUC, sensitivity, specificity and the cutoff value, respectively, for differentiating low- from high-grade gliomas for ADC, D and f, and differentiating high- from low-grade gliomas for D* were as follows: ADC, 0.926, 100%, 82.8%, and $0.7 \times 10^{-3} \text{ mm}^2/\text{sec}$; D, 0.942, 92.3%, 86.2%, and $0.623 \times 10^{-3} \text{ mm}^2/\text{sec}$; f, 0.902, 92.3%, 86.2%, and 35.3%; D*, 0.798, 79.3%, 84.6%, and $0.303 \times 10^{-3} \text{ mm}^2/\text{sec}$. The IVIM DWI demonstrates efficacy in differentiating the low- from high-grade gliomas.

Glioma remains the most common primary malignant brain tumor worldwide¹. Glioma is classified into 4 grades, with worse prognosis for more advanced grades². Previous studies have suggested that different therapeutic strategies should be applied for gliomas at different grades. For example, surgical resection is suggested to be the best approach for low-grade gliomas^{3,4}, whereas adjuvant chemotherapy and radiotherapy after resection are shown to produce benefits for high-grade glioma patients^{5,6}. Glioma grading before the operation is therefore of important clinical significance for guiding the grade-dependent therapeutic strategy.

Magnetic resonance imaging (MRI) has played important roles in preoperative grading and optimizing therapies⁷. However, current grading of gliomas with conventional MRI remains unsatisfactory. As an improved MRI technique, diffusion-weighted imaging (DWI) is considered the most sensitive for early pathological changes and therefore can potentially be useful in evaluating the features of gliomas^{7,8}. To overcome a limitation of DWI, which is that perfusion can substantially confound diffusion measurements because of the incoherent motion of blood, intravoxel incoherent motion (IVIM) based on DWI is proposed^{9,10}. Although the IVIM MRI technique has been suggested to be useful in the diagnosis and differential diagnosis of salivary gland, pancreas, renal, liver and breast tumors^{11–15}, it remains largely unknown whether IVIM MRI can be used to effectively grade glioma and which criteria for parameters should be applied. Although a recent study reported a first attempt to address this issue¹⁶, only parameter differences between low- and high-grade gliomas were reported, and there was no information regarding the suitable cutoff values of the suggested differentiating parameters. Therefore, we conducted the current retrospective study to further assess the relationship between parameters (apparent diffusion coefficient (ADC), slow diffusion coefficient (D), fast diffusion coefficient (D*), and fraction of fast

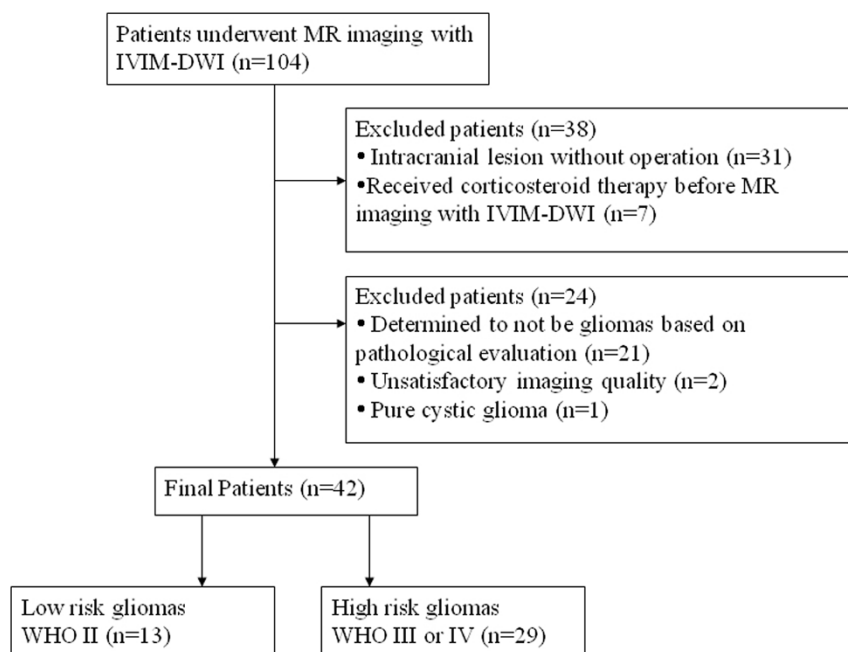


Figure 1 | Flow diagram for the patient selection process.

ADC (f) based on IVIM models and the glioma grades and to determine the cutoff values of suggested parameters for differentiating high- from low-grade gliomas.

Results

The histological diagnosis of excised tumors from the 42 patients included in this study (Figure 1) demonstrated that 29 patients had high-grade gliomas (12 had WHO grade IV glioblastoma, 13 had WHO grade III anaplastic astrocytoma, 1 had WHO grade III gliomatosis cerebri and 3 had WHO grade III anaplastic oligodendroglioma), and 13 had low-grade gliomas (6 had WHO grade II astrocytoma and 7 had WHO grade II oligodendroglioma). The descriptive statistics of the IVIM parameters (ADC, D , D^* and f) in the tumor sites and healthy white matter sites between patients with low- and high-grade gliomas are shown in Table 1 and Table 2, respectively. In healthy white matter sites between patients with low- and high-grade gliomas, these 4 parameters demonstrated comparable results with no significant differences ($P > 0.05$) (Table 2): the ADC mean value was $0.551 \times 10^{-3} \text{ mm}^2/\text{sec}$ in low-grade (WHO grade II) gliomas and $0.534 \times 10^{-3} \text{ mm}^2/\text{sec}$ in high-grade (WHO grade III-IV) gliomas ($P = 0.142$); the mean value of D was $0.441 \times 10^{-3} \text{ mm}^2/\text{sec}$ in low-grade gliomas and $0.424 \times 10^{-3} \text{ mm}^2/\text{sec}$ in high-grade gliomas ($P = 0.157$); the mean value of f was 0.300 in low-grade gliomas and 0.294 in high-grade gliomas ($P = 0.576$); and the mean value of D^* was $2.310 \times 10^{-3} \text{ mm}^2/\text{sec}$ in low-grade gliomas and $2.355 \times 10^{-3} \text{ mm}^2/\text{sec}$ in high-grade gliomas ($P = 0.157$). By contrast, in tumor sites between patients with low- and high-grade gliomas, we detected significant differences for all 4 parameters (Table 1). Specifically, the mean value of ADC was higher for the

low-grade gliomas compared with high-grade gliomas (0.906×10^{-3} vs $0.618 \times 10^{-3} \text{ mm}^2/\text{sec}$, $P < 0.001$); higher mean values of D and f were also observed for the low-grade gliomas (0.756×10^{-3} vs $0.506 \times 10^{-3} \text{ mm}^2/\text{sec}$, $P < 0.001$; 0.477 vs 0.290 , $P < 0.001$, respectively), whereas for D^* , the mean value was higher for the high-grade patients than the low-grade patients (2.706×10^{-3} vs $2.150 \times 10^{-3} \text{ mm}^2/\text{sec}$, $P = 0.013$). The box plots of these parameters in the 2 categories of gliomas clearly demonstrate these patterns (Figure 2).

Figure 3 demonstrates the ROC curves for the grading performances of the four parameters (ADC, D , f , and D^*), specifically, differentiating the low- from high- grade gliomas for ADC, D , and f , and differentiating the high- from low-grade gliomas for D^* . The values of AUC, sensitivity, specificity, as well as the suggestive cutoff values for each parameter are shown in Table 3. Briefly, with an AUC of 0.926, the ADC parameter had 100% sensitivity and 82.8% specificity for identifying low-grade gliomas at the cutoff value of $0.7 \times 10^{-3} \text{ mm}^2/\text{sec}$. The AUC for parameter D was 0.942, and 92.3% sensitivity and 86.2% specificity was achieved for identifying low-grade gliomas at the cutoff value of $0.623 \times 10^{-3} \text{ mm}^2/\text{sec}$. For parameter f , with an AUC of 0.902, 92.3% sensitivity and 86.2% specificity was achieved at the cutoff value of 35.3%. Additionally, D^* achieved an AUC of 0.798, and the cutoff value of $2.303 \times 10^{-3} \text{ mm}^2/\text{sec}$ exhibited a sensitivity of 79.3% and a specificity of 84.6% for identifying high-grade gliomas.

Discussion

In the current study, we evaluated whether the IVIM MRI could be used preoperatively to grade gliomas. We detected significant differ-

Table 1 | IVIM-derived parameters in the tumor sites in low- and high-grade gliomas

	LGG	HGG	P-value*
ADC ($\times 10^{-3} \text{ mm}^2 / \text{sec}$)	0.906 ± 0.110	0.618 ± 0.142	0.000
D ($\times 10^{-3} \text{ mm}^2 / \text{sec}$)	0.756 ± 0.110	0.506 ± 0.117	0.000
D^* ($\times 10^{-3} \text{ mm}^2 / \text{sec}$)	2.150 ± 0.423	2.706 ± 0.852	0.013
f	0.477 ± 0.130	0.290 ± 0.096	0.000

Note: LGG denotes low-grade gliomas, HGG denotes high-grade gliomas.

*The P values were the comparison of the parameters between low- and high- grade gliomas.



Table 2 | IVIM-derived parameters in the normal white matter between low- and high-grade gliomas

	LGG	HGG	P-value*
ADC ($\times 10^{-3}$ mm ² /sec)	0.551 \pm 0.023	0.534 \pm 0.038	0.142
D ($\times 10^{-3}$ mm ² /sec)	0.441 \pm 0.026	0.424 \pm 0.039	0.157
D* ($\times 10^{-3}$ mm ² /sec)	2.310 \pm 0.351	2.355 \pm 0.260	0.647
f	0.300 \pm 0.032	0.294 \pm 0.027	0.576

Note: LGG denotes low-grade gliomas, HGG denotes high-grade gliomas.

*The P values were the comparison of the parameters in normal white matter between low- and high grade gliomas.

ences in parameters ADC, D, D*, and f between low- and high-grade gliomas. We also determined the most appropriate cutoff values for each suggested parameter, which could potentially be used in clinical practice regarding preoperatively grading gliomas, if validated in larger studies.

The ADC value can potentially reveal the differences in cellularity and nuclear atypia of gliomas¹⁷. Theoretically, high cellularity in advanced gliomas may impede free water diffusion and thus lead to a decreased ADC value. In a study by Higano et al., the minimum ADC varied significantly between WHO grade III ($(1.06 \pm 0.21) \times 10^{-3}$ mm²/sec) and WHO grade IV gliomas ($(0.83 \pm 0.14) \times 10^{-3}$ mm²/sec)¹⁸. Another study also revealed a significantly higher frequency of low ADC values in high- compared with low-grade gliomas¹⁹. In addition, parameter D was shown to be inversely correlated with cell density¹⁷. In the current study, we found that the

ADC and D values were significantly lower in high-grade gliomas compared with low-grade gliomas ($P < 0.001$), which confirmed previous findings²⁰.

Interestingly, our findings are inconsistent with another recently published study, in which ADC and D did not demonstrate significant differences between low- and high-grade gliomas¹⁶. One possible explanation for the deviation can be that different b values were used. Research has indicated that the accuracy of IVIM parameter calculation is affected by b values^{9,20}. In the current study, 13 b values were used, including 5 ranging from 0 to 200 sec/mm² and 8 ranging from 300 to 3500 sec/mm², which is markedly different from the previous study in which 11 b values ranging from 0 to 200 sec/mm² and 3 ranging from 700 to 1300 sec/mm² were used¹⁶. Another possible explanation is the different definition of ROI applied in these two studies. In the previous study, the ROI was

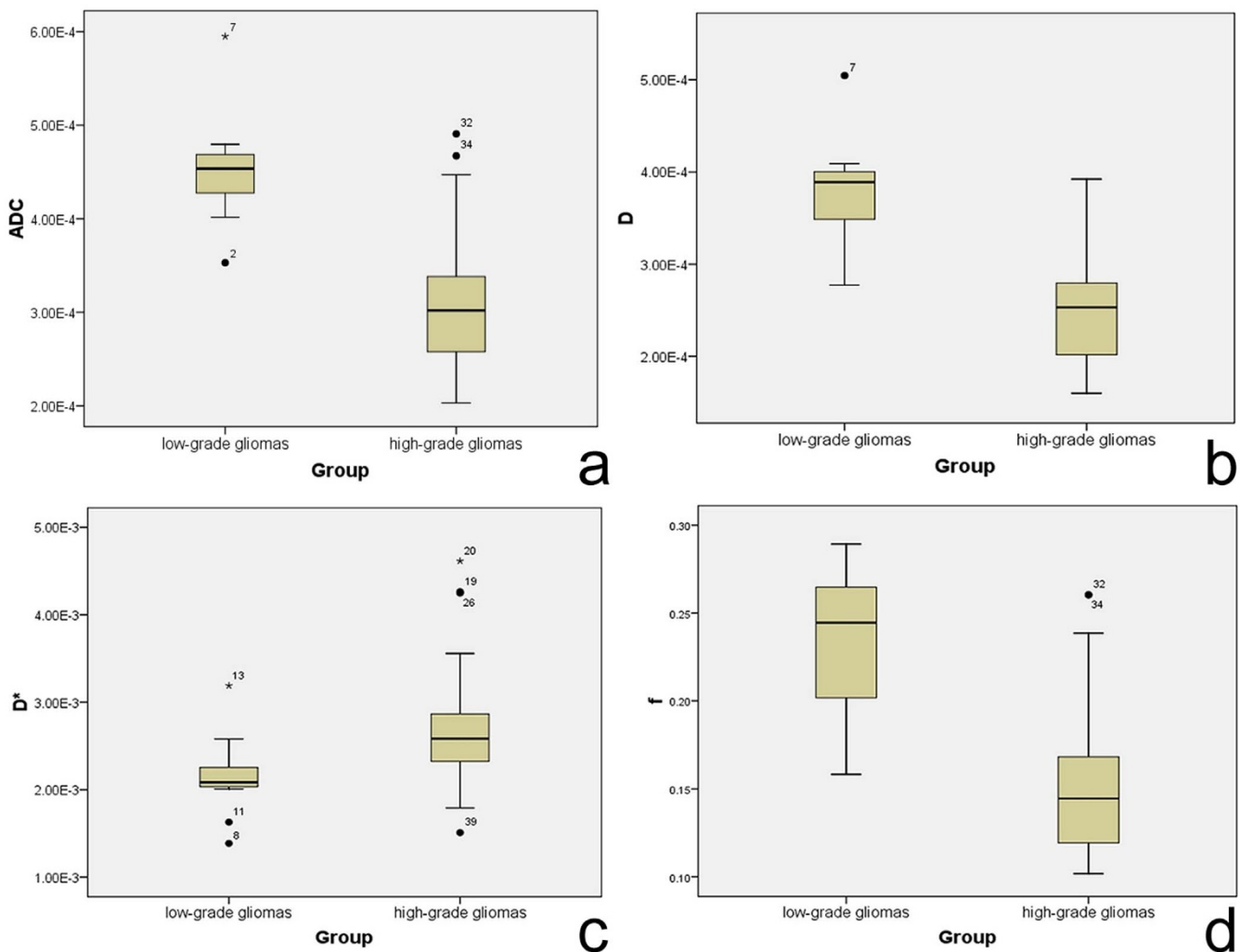


Figure 2 | Box plots for values of ADC, D, D*, and f in high- and low-grade gliomas.

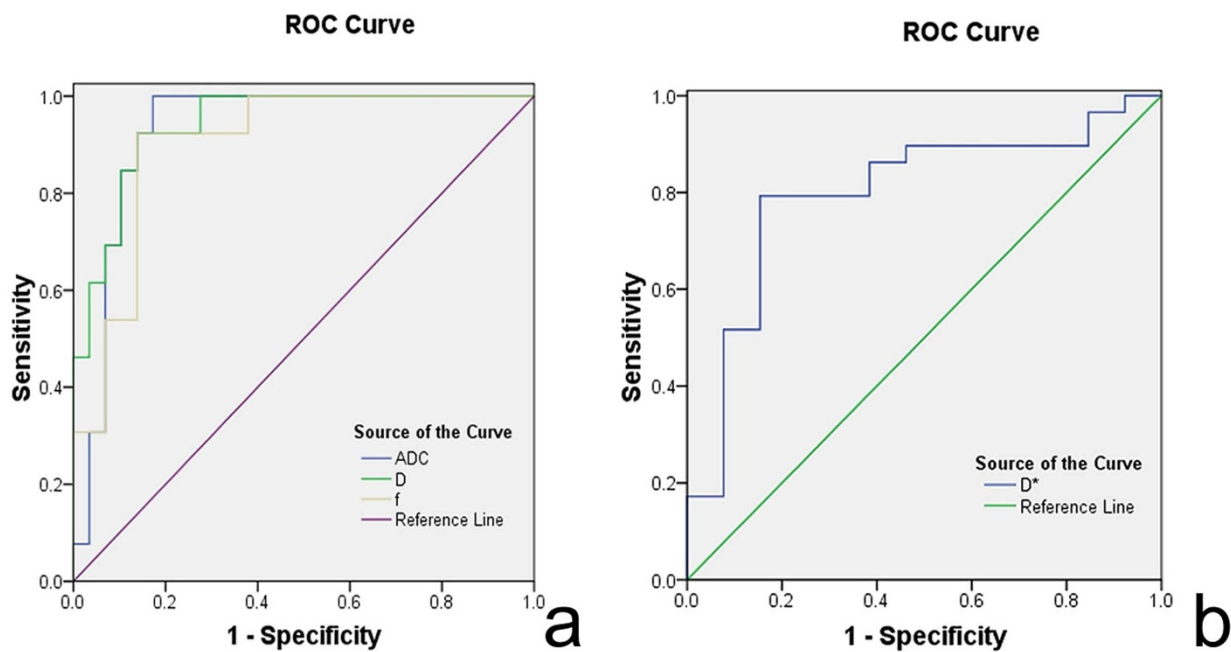


Figure 3 | ROC curve for differentiating the performance of the four parameters (ADC, D, D*, and f), specifically, differentiating the low- from high-grade gliomas for ADC, D and f, and identifying the high- from low- grade gliomas for D*.

placed on the tumor area with the largest diameter encompassing as much solid tumor area as possible¹⁶. However, because of the heterogeneous inner structure of glioma, especially anaplastic glioma and glioblastoma, we argue the most malignant portion of tumor may be more appropriate for calculating the parameters²¹. In the current study, ROI included the tumor solid parts with the highest signal intensity on DW imaging ($b=1000 \text{ sec/mm}^2$) and the relatively low ADC values of the corresponding areas on ADC map, based on the rationale of using the minimum ADC value measurements to sample the highest tumor cell attenuation or the most proliferative portions of the tumor. We noted that another study used a similar method of determining ROI and suggested that measuring the minimum ADC could provide diagnostic information for the preoperative grading of supratentorial astrocytomas²¹.

The degree of neovascularization is critical in assessing tumor grade and malignancy²². Malignant gliomas are characterized by increased angiogenesis, which is a marker of the histological grading system²³. The parameter D^* within the IVIM model is influenced by microvessel density (MVD) within the tumor, which is associated with an average length of capillaries and blood flow velocities⁹. In the current study, we demonstrated that D^* was significantly higher in high-grade than in low-grade gliomas, which is consistent with the MVD theory⁹. Previous studies have suggested that the relative cerebral blood volume (rCBV) value is correlated with the grade and vascularity in gliomas^{24,25}. Usually, low-grade gliomas show no increase in tumor rCBV, whereas high-grade gliomas demonstrate high rCBV that in some cases even extends outside the contrast-enhancing portions of the tumor²⁶.

The parameter f represents the fraction of the fast diffusion component and is affected by the abundance of capillaries. In this ana-

lysis, we detected that f was significantly lower in high-grade gliomas, which is inconsistent with findings in several other studies^{16,27}. Several potential reasons may explain this difference. The instruments used in these studies are not consistent, and different b values were used. Because the lower b -values were more important for calculating pseudodiffusion²⁸, the b value might influence the accuracy of the f value measurements. Additionally, as discussed above, in our study, we determined ROI to include the tumor solid parts with the highest signal intensity on DW imaging, which is in contrast to other studies. The highest cellularity density and the nuclear cytoplasmic ratio as well as relatively fewer mesenchymal components are revealed in anaplastic gliomas and glioblastomas²³, which can potentially explain the findings involving f ^{16,27}.

In the current study, we also assessed the diagnostic efficacy of IVIM parameters in differentiating glioma grades. Although the optimal b values remain unknown, we demonstrated that ADC, D, D^* , and f could achieve relatively high AUC in grading gliomas preoperatively. It was indicated that a cutoff value of $0.7 \times 10^{-3} \text{ mm}^2/\text{sec}$ for ADC, $0.623 \times 10^{-3} \text{ mm}^2/\text{sec}$ for D, and 35.3% for f could produce relatively satisfactory sensitivity and specificity for identifying low- from high-grade gliomas. The combined evaluation of these three values may provide a better estimation for the preoperative glioma grading.

One important consideration of using the IVIM technique based on DW MRI is obtaining reliable and repeatable data from patients. In our study, to ensure data accuracy, we obtained data from healthy white matter sites in patients. Analysis revealed no significant difference for each parameter between low- and high-grade gliomas (as shown in table 2), which suggested the reliability of the obtained data in our study.

Table 3 | ROC curve

	AUC	P value	Sensitivity (%)	Specificity (%)	Cutoff value
ADC ($\times 10^{-3} \text{ mm}^2 / \text{sec}$)	.926	.000	100.0	82.8	.700
D ($\times 10^{-3} \text{ mm}^2 / \text{sec}$)	.942	.000	92.3	86.2	.623
D^* ($\times 10^{-3} \text{ mm}^2 / \text{sec}$)	.798	.002	79.3	84.6	2.303
f (%)	.902	.000	92.3	86.2	.353

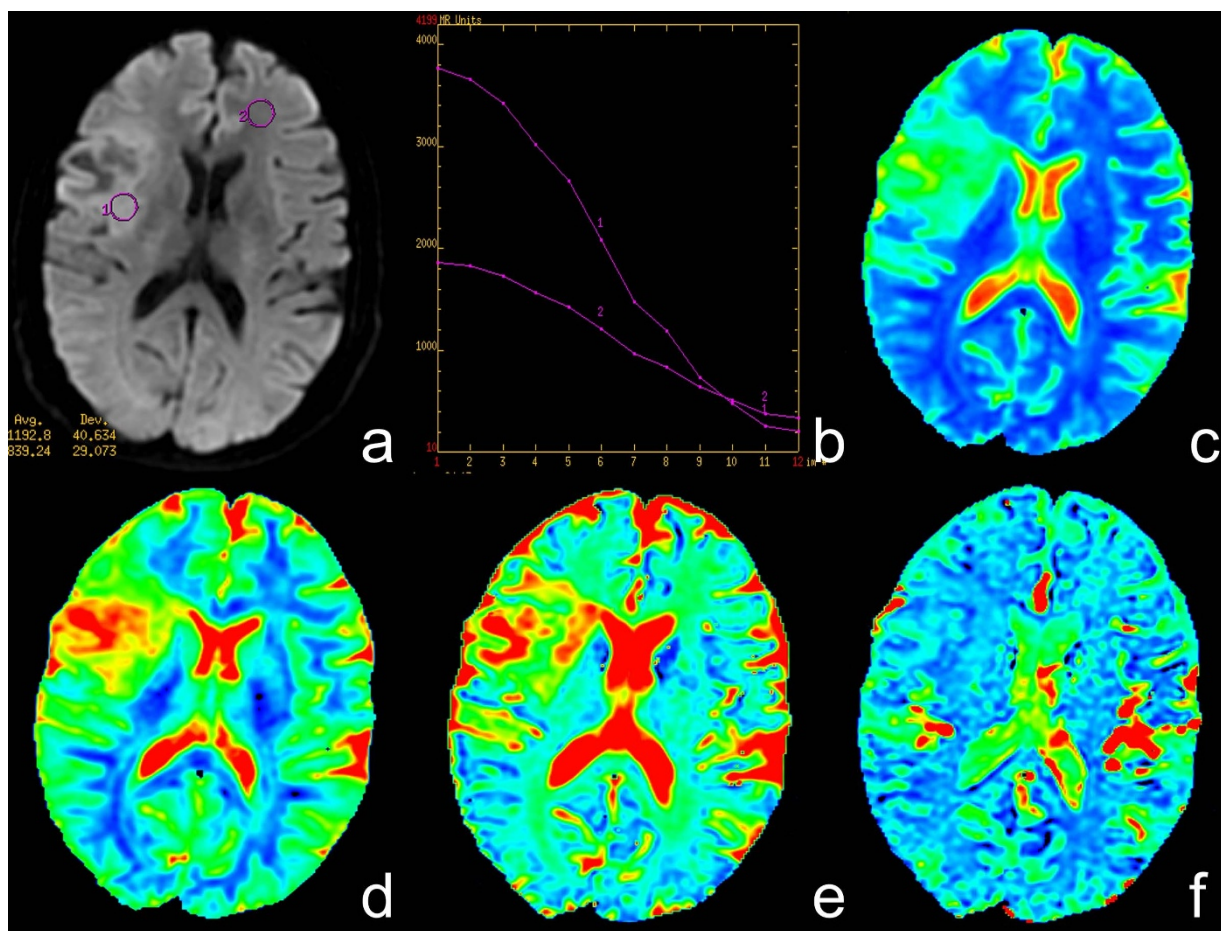


Figure 4 | A case of low-grade glioma. (a) Axial diffusion-weighted trace image ($b=1000 \text{ sec/mm}^2$). (b) The bi-exponential fitting of the diffusion signal decay over a wide-range of b values (up to 3,500). (c) Axial apparent diffusion coefficient (ADC) map. (d) The D map. (e) The f map. (f) The D^* map. The DWI shows a mild hyperintense mass (ROI 1) on the right frontal-temporal region in a patient with grade II glioma. On the ADC and D map, the region of tumor is confirmed as higher signal intensity (increased ADC value, encoded in a green–yellow–red color schema) compared to the healthy white matter (ROI 2). The f map demonstrates a higher perfusion fraction region compared to the healthy white matter. The D^* map shows a slightly decreased fast-diffusion values in the tumor tissue compared to the healthy white matter.

Several concerns should be considered in interpreting our findings. First, hand-drawn ROIs were used in the current study. Because the nests of tumor cells tend to be heterogeneously distributed, a measurement of ADC values by manual drawing of the ROIs on the DWI (trace image) may introduce sampling bias. Second, the b values ranging from 0 to 200 sec/mm^2 are limited in our study, which may influence the accurate assessment of f and D^* . However, the optimal number of lower b -values for IVIM remains undetermined, and further research is warranted to clarify this issue.

To the best of our knowledge, this is the largest study to date that evaluated IVIM modelling based on DW MRI in differentiating low-from high-grade gliomas. Our study clearly suggests that several parameters from IVIM modelling, including ADC, D , D^* , and f , could potentially serve as non-invasive predictors for the preoperative grading of gliomas.

Methods

Participants. This single-center retrospective study was approved by the Ethics Committee of Tangdu Hospital of the Fourth Military Medical University, and informed consents were obtained from all participants. This study was conducted in accordance with the Declaration of Helsinki. Between September 2013 and May 2014, 104 consecutive patients with suspected intracranial occupying lesions underwent routine MRI, IVIM DWI, as well as contrast-enhanced MRI of the brain. Of these, 62 subjects were excluded as follows: 1, the histopathological grades were not available because operations were not performed ($n=31$); 2, corticosteroid therapy was administered before MR imaging with IVIM-DWI ($n=7$); 3, the lesion was

determined not to be a glioma based on pathological evaluation ($n=21$); 4, the image quality was unsatisfactory ($n=2$); and 5, a pure cystic glioma was observed ($n=1$). The final study population contained 42 patients (25 men and 17 women; mean age, 47 years; age range, 19–77 years) with newly diagnosed glioma.

Brain MR imaging. The whole brain MRI examinations were performed on a 3.0-T MRI system (MR750, GE Healthcare, Milwaukee, WI, USA) with a standard receive-only head coil. Conventional MRI, DWI with 13 b -values ($0\text{--}3500 \text{ s/mm}^2$) and contrast-enhanced MRI were performed in regular sequence during the same examination. Conventional MRI sequences included T1-weighted spin echo in the transverse plane (TR/TE, 1,750 ms/24 ms; matrix size, 256×256 ; field of view, $24 \times 24 \text{ cm}$; number of excitation, 1; slice thickness, 5 mm; gap, 1.5 mm), T2-weighted fast spin echo in the transverse planes (TR/TE, 4,247 ms/93 ms; matrix size, 512×512 ; field of view, $24 \times 24 \text{ cm}$; number of excitation, 1; slice thickness, 5 mm; gap, 1.5 mm) and sagittal planes (TR/TE, 10,639 ms/96 ms; matrix size, 384×384 ; field of view, $24 \times 24 \text{ cm}$; number of excitation, 2; slice thickness, 5 mm; gap, 1.0 mm), and fluid-attenuated inversion recovery (FLAIR) in the transverse plane (TR/TE, 8,000 ms/165 ms; matrix size, 256×256 ; field of view, $24 \text{ cm} \times 24 \text{ cm}$; number of excitation, 1; slice thickness, 5 mm; gap, 1.5 mm).

The IVIM DWI sequence was performed prior to the injection of Gd. Thirteen b values (0, 30, 50, 100, 200, 300, 500, 800, 1000, 1500, 2000, 3000 and 3500 s/mm^2) were applied with a single-shot diffusion-weighted spin-echo echo-planar sequence. The lookup table of gradient directions was modified to allow multiple b value measurements in one series. Parallel imaging was used with an acceleration factor of 2. A local shim box covering the whole brain was applied to minimize susceptibility artifacts. In total, 20 axial slices covering the entire brain were obtained with a 24-cm field of view, 5 mm slice thickness, 1.5 mm slice gap, 3,000 ms TR, Minimum TE, 128×128 matrix. The total scan time was 5 min and 45 s.

Finally, a contrast-enhanced T1-weighted spin echo sequence was performed in the transverse, sagittal, and coronal planes (TR/TE, 1850 ms/24 ms for transverse

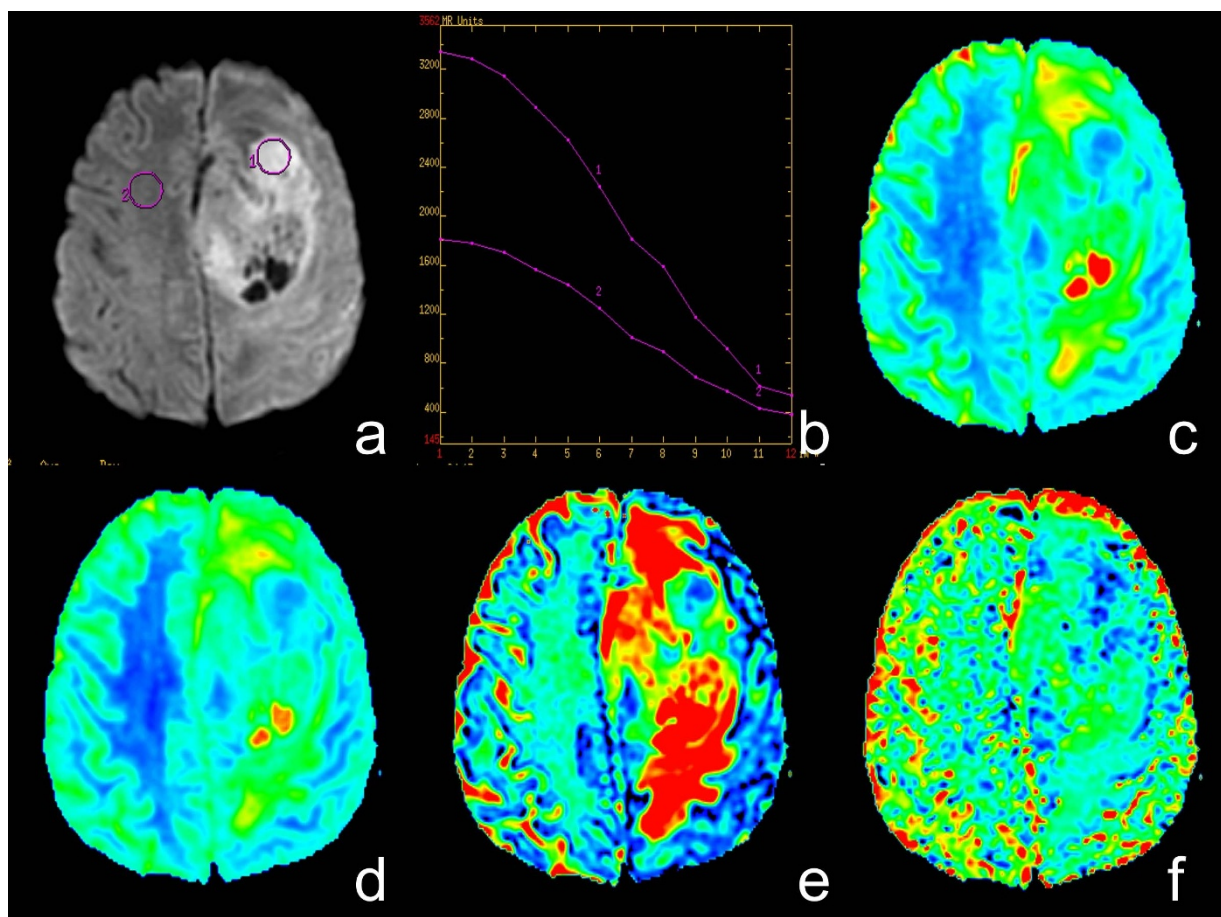


Figure 5 | A case of high-grade glioma. (a) Axial diffusion-weighted trace image ($b=1000 \text{ sec/mm}^2$). (b) The bi-exponential fitting of the diffusion signal decay over a wide-range of b values (up to 3,500). (c) Axial apparent diffusion coefficient (ADC) map. (d) The D map. (e) The f map. (f) The D^* map. The DWI shows inhomogeneous signal intensity mass on the left frontal-parietal lobe in a patient with grade IV glioma, with significantly high signal intensity (ROI 1) in tumor. On the ADC and D map, the area of restricted diffusion is confirmed as an isointense lesion (decreased ADC value, encoded in a blue color) compared to the healthy white matter (ROI 2). The f map demonstrates a higher perfusion fraction region compared to the healthy white matter. The D^* map shows a slightly decreased fast-diffusion values in the tumor tissue compared to the healthy white matter.

plane and 1750 ms/24 ms for sagittal and coronal planes; other parameters were the same as conventional MRI) following a bolus injection of 0.1 mmol/kg of gadodiamide injection (Omniscan; GE Healthcare, Co.Cork, Ireland).

IVIM DW MRI analysis. According to IVIM, the relationship between signal variation and b values can be expressed by using Equation (1)⁹:

$$S_b/S_0 = f \exp(-b D^*) + (1-f) \exp(-b D) \quad (1)$$

where S_0 and S_b are the signal intensities at a b value of 0 sec/mm^2 and each b value other than 0 sec/mm^2 , respectively; D is the true diffusion coefficient that reflects random motion of intra- and intercellular water molecules (slow component of diffusion); f is the fraction of the diffusion linked to microcirculation, and D^* is the diffusion parameter representing incoherent microcirculation within the voxel (perfusion-related diffusion, or fast component of diffusion).

Considering that D^* is significantly greater than $D^{9,10}$, the influence of D^* on signal decay can be neglected for b values greater than 200 sec/mm^2 . Equation (1) can then be simplified, and the estimation of D can be obtained by using only b values greater than 200 sec/mm^2 , with a simple linear fit equation (2):

$$S_b/S_0 = \exp(-b D) \quad (2)$$

Hence, for high b values (300, 500, 800, 1000, 1500, 2000, 3000 and 3500 sec/mm^2) S_b was first fitted to equation (2) using a linear model, and the true diffusion coefficient D was calculated. The f and D^* values were calculated by using a nonlinear regression algorithm based on equation (1).

The ADC value was calculated by fitting the b_0 image and DWIs at each b value other than 0 sec/mm^2 into the conventional ADC equation (Eq. (3))⁹:

$$S_b/S_0 = \exp(-b \text{ADC}) \quad (3)$$

Magnetic Resonance Imaging Data Processing and Quantitative Analysis

All data were analyzed and processed on a GE ADW4.6 workstation. The mean values of all IVIM parameters were measured independently by two experienced radiologists. First, they reviewed the conventional plain and contrast-enhanced MRI images carefully to determine the solid part of each tumor. Next, the multi- b -value data were analyzed using a MADC program. A freehand ROI was placed to cover as much of the solid part of the tumors as possible; a freehand ROI was placed to include the solid tumor parts with the highest signal intensity on DW image ($b=1000 \text{ sec/mm}^2$) and the relatively low ADC values of the corresponding areas on the ADC map to avoid large vessels and hemorrhagic, calcified, cystic and necrotic areas (as shown in Figure 4.a or Figure 5.a). The mean ROI area of the lesions was $135.5 \pm 92.7 \text{ mm}^2$ (range, 45.0–374.0 mm^2). For the contralateral healthy appearing white matter, standardized ROIs (the same size as the ROI of the lesions) were placed. The parameter maps of IVIM were generated automatically by the MADC program (as shown in Figure 4 or Figure 5), and the mean ADC, D , D^* , and f values in the ROIs were obtained, respectively.

Statistical analysis. Numerical variables were denoted as the mean and standard deviation. Parameters ADC, D , D^* , and f in healthy white matter and tumor sites were tested for differences between the low-grade (WHO II) and the high-grade gliomas (WHO III and IV) by using ANOVA. Receiver operating characteristic (ROC) analyses were performed to determine the optimal thresholds for differentiating the low-grade (WHO II) from the high-grade gliomas (WHO III and IV) by ADC, D , D^* , and f value. In addition, the sensitivity, specificity, and area under curve (AUC) for identifying low-grade gliomas were calculated in each case, except for D^* when high-grade gliomas were differentiated. $P < 0.05$ indicated a statistically significant difference. SPSS17.0 software (SPSS Inc, Chicago, IL, USA) was used for all statistical analyses.

- Omuro, A. & DeAngelis, L. M. Glioblastoma and other malignant gliomas: a clinical review. *JAMA* **310**, 1842–1850, doi:10.1001/jama.2013.280319 (2013).



2. Louis, D. N. *et al.* The 2007 WHO classification of tumours of the central nervous system. *Acta Neuropathol* **114**, 97–109, doi:10.1007/s00401-007-0243-4 (2007).
3. Jakola, A. S. *et al.* Comparison of a strategy favoring early surgical resection vs a strategy favoring watchful waiting in low-grade gliomas. *JAMA* **308**, 1881–1888, doi:10.1001/jama.2012.12807 (2012).
4. Nageswara Rao, A. A. & Packer, R. J. Advances in the management of low-grade gliomas. *Curr Oncol Rep* **16**, 398, doi:10.1007/s11912-014-0398-9 (2014).
5. Stewart, L. A. Chemotherapy in adult high-grade glioma: a systematic review and meta-analysis of individual patient data from 12 randomised trials. *Lancet* **359**, 1011–1018 (2002).
6. Vern-Gross, T. Z. *et al.* Prospective evaluation of local control and late effects of conformal radiation therapy in children, adolescents, and young adults with high-grade glioma. *Neuro Oncol*, doi:10.1093/neuonc/nou101 (2014).
7. Kao, H. W., Chiang, S. W., Chung, H. W., Tsai, F. Y. & Chen, C. Y. Advanced MR imaging of gliomas: an update. *Biomed Res Int* **2013**, 970586, doi:10.1155/2013/970586 (2013).
8. Kono, K. *et al.* The role of diffusion-weighted imaging in patients with brain tumors. *AJNR Am J Neuroradiol* **22**, 1081–1088 (2001).
9. Luciani, A. *et al.* Liver cirrhosis: intravoxel incoherent motion MR imaging--pilot study. *Radiology* **249**, 891–899, doi:10.1148/radiol.2493080080 (2008).
10. Le Bihan, D. *et al.* Separation of diffusion and perfusion in intravoxel incoherent motion MR imaging. *Radiology* **168**, 497–505, doi:10.1148/radiology.168.2.3393671 (1988).
11. Sigmund, E. E. *et al.* Intravoxel incoherent motion imaging of tumor microenvironment in locally advanced breast cancer. *Magn Reson Med* **65**, 1437–1447, doi:10.1002/mrm.22740 (2011).
12. Chandarana, H. *et al.* Diffusion-weighted intravoxel incoherent motion imaging of renal tumors with histopathologic correlation. *Invest Radiol* **47**, 688–696, doi:10.1097/RLI.0b013e31826a0a49 (2012).
13. Yoon, J. H. *et al.* Evaluation of hepatic focal lesions using diffusion-weighted MR imaging: comparison of apparent diffusion coefficient and intravoxel incoherent motion-derived parameters. *J Magn Reson Imaging* **39**, 276–285, doi:10.1002/jmri.24158 (2014).
14. Lemke, A. *et al.* Differentiation of pancreas carcinoma from healthy pancreatic tissue using multiple b-values: comparison of apparent diffusion coefficient and intravoxel incoherent motion derived parameters. *Invest Radiol* **44**, 769–775, doi:10.1097/RLI.0b013e3181b62271 (2009).
15. Sumi, M. *et al.* Salivary gland tumors: use of intravoxel incoherent motion MR imaging for assessment of diffusion and perfusion for the differentiation of benign from malignant tumors. *Radiology* **263**, 770–777, doi:10.1148/radiol.12111248 (2012).
16. Bisdas, S. *et al.* Intravoxel incoherent motion diffusion-weighted MR imaging of gliomas: feasibility of the method and initial results. *Neuroradiology* **55**, 1189–1196, doi:10.1007/s00234-013-1229-7 (2013).
17. Sadeghi, N. *et al.* Effect of hydrophilic components of the extracellular matrix on quantifiable diffusion-weighted imaging of human gliomas: preliminary results of correlating apparent diffusion coefficient values and hyaluronan expression level. *AJR Am J Roentgenol* **181**, 235–241, doi:10.2214/ajr.181.1.1810235 (2003).
18. Higano, S. *et al.* Malignant astrocytic tumors: clinical importance of apparent diffusion coefficient in prediction of grade and prognosis. *Radiology* **241**, 839–846, doi:10.1148/radiol.2413051276 (2006).
19. Wen, P. Y. & Kesari, S. Malignant gliomas in adults. *N Engl J Med* **359**, 492–507, doi:10.1056/NEJMra0708126 (2008).
20. Iima, M. *et al.* Characterization of glioma microcirculation and tissue features using intravoxel incoherent motion magnetic resonance imaging in a rat brain model. *Invest Radiol* **49**, 485–490, doi:10.1097/RLI.0000000000000040 (2014).
21. Lee, E. J. *et al.* Preoperative grading of presumptive low-grade astrocytomas on MR imaging: diagnostic value of minimum apparent diffusion coefficient. *AJNR Am J Neuroradiol* **29**, 1872–1877, doi:10.3174/ajnr.A1254 (2008).
22. Kang, Y. *et al.* Gliomas: Histogram analysis of apparent diffusion coefficient maps with standard- or high-b-value diffusion-weighted MR imaging--correlation with tumor grade. *Radiology* **261**, 882–890, doi:10.1148/radiol.11110686 (2011).
23. Plate, K. H., Breier, G., Weich, H. A. & Risau, W. Vascular endothelial growth factor is a potential tumour angiogenesis factor in human gliomas in vivo. *Nature* **359**, 845–848, doi:10.1038/359845a0 (1992).
24. Thompson, G., Mills, S. J., Coope, D. J., O'Connor, J. P. & Jackson, A. Imaging biomarkers of angiogenesis and the microvascular environment in cerebral tumours. *Br J Radiol* **84 Spec No 2**, S127–144, doi:10.1259/bjr/66316279 (2011).
25. Shin, J. H. *et al.* Using relative cerebral blood flow and volume to evaluate the histopathologic grade of cerebral gliomas: preliminary results. *AJR Am J Roentgenol* **179**, 783–789, doi:10.2214/ajr.179.3.1790783 (2002).
26. Hu, L. S. *et al.* Correlations between perfusion MR imaging cerebral blood volume, microvessel quantification, and clinical outcome using stereotactic analysis in recurrent high-grade glioma. *AJNR Am J Neuroradiol* **33**, 69–76, doi:10.3174/ajnr.A2743 (2012).
27. Federau, C., Meuli, R., O'Brien, K., Maeder, P. & Hagmann, P. Perfusion measurement in brain gliomas with intravoxel incoherent motion MRI. *AJNR Am J Neuroradiol* **35**, 256–262, doi:10.3174/ajnr.A3686 (2014).
28. Cohen, A. D., Schieke, M. C., Hohenwarter, M. D. & Schmainda, K. M. The effect of low b-values on the intravoxel incoherent motion derived pseudodiffusion parameter in liver. *Magn Reson Med*, doi:10.1002/mrm.25109 (2014).

Acknowledgments

We would like to thank Dr. Dandan Zheng of GE Healthcare Greater China for her helpful comments during the revision of this manuscript.

Author contributions

Y.-C.H., L.-F.Y., L.W., W.W. and G.-B.C. participated in the study design. Y.-C.H., L.-F.Y., P.D., B.-Y.C., L.W., S.-M.W., Y.H., Q.T., Y.Y., T.-Y.X. collected the data; Y.-C.H., L.W. and W.W. analyzed the data; all authors participated in the interpretation of the data; Y.-C.H. and L.W. prepared the first draft of the manuscript; all authors revised and approved the manuscript.

Additional information

Competing financial interests: T-YX is an employee of GE healthcare Greater China. All other authors declare no conflict of interests.

How to cite this article: Hu, Y.-C. *et al.* Intravoxel incoherent motion diffusion-weighted MR imaging of gliomas: efficacy in preoperative grading. *Sci. Rep.* **4**, 7208; DOI:10.1038/srep07208 (2014).



This work is licensed under a Creative Commons Attribution-NonCommercial-ShareAlike 4.0 International License. The images or other third party material in this article are included in the article's Creative Commons license, unless indicated otherwise in the credit line; if the material is not included under the Creative Commons license, users will need to obtain permission from the license holder in order to reproduce the material. To view a copy of this license, visit <http://creativecommons.org/licenses/by-nc-sa/4.0/>